How to Cite: Muslimova, I.B., Khairusheva, A.B., Izbassar, K.A., Bekbol, Zh.A., Lissovskaya, L.I. & Korolkov, I.V. (2026). Surface-Enhanced Raman Detection of Low-Concentration Methylene Blue Using Nanoparticles Functionalized with 12-Mercaptododecanoic Acid. *Eurasian Journal of Chemistry, 31, 3(123), 53–65.* https://doi.org/10.31489/2959-0663/3-26-4

Article

Received: 20 May 2026 | Revised: 12 August 2026 |
Accepted: 20 August 2026 | Published online: 28 August 2026

UDC 544.42+519.242.7

https://doi.org/10.31489/2959-0663/3-26-4

Indira B. Muslimova[1*], Ainur B. Khairusheva[2], Kairat A. Izbassar[2], Zhangali A. Bekbol[2], Lana I. Lissovskaya[1,2], Ilya V. Korolkov[1,2]

[1]*Institute of Nuclear Physics ARKAE, Almaty, Kazakhstan*
[2]*L.N. Gumilyov Eurasian National University, Astana, Kazakhstan*
*(*Corresponding author's e-mail: i.muslimova@inp.kz)*

Surface-Enhanced Raman Detection of Low-Concentration Methylene Blue Using Nanoparticles Functionalized with 12-Mercaptododecanoic Acid

The development of sensitive and magnetically recoverable SERS substrates is of interest for the detection of organic pollutants at low concentrations. In this study, Fe_3O_4-CA@Au-12-MDA nanoparticles were synthesized for use as a SERS substrate in the detection of methylene blue dye within a concentration range of 10^{-2}-10^{-7} M. The Fe_3O_4 magnetic nanoparticles were modified with citric acid, followed by gold deposition and surface functionalization with 12-mercapto-dodecanoic acid. The stepwise modification of the nanoparticles was confirmed by FTIR, SEM-EDX and XRD, which revealed the presence of Au and organic functional groups whilst preserving the crystalline structure of Fe_3O_4. The Fe_3O_4-CA@Au-12-MDA-based SERS substrate exhibited signal enhancement compared to conventional Raman spectroscopy. For the characteristic bands at 1623 and 1396 cm^{-1}, the approximate EF values reached 0.11×10^5 and 0.15×10^5, respectively, corresponding to 5.95- and 5.40 times signal enhancement. The estimated LOD values calculated using the 3σ criterion were 4.05×10^{-8} and 5.97×10^{-8} M for the respective bands. The calibration curves demonstrated good linearity with R^2 values of 0.94-0.99 for SERS measurements. The results obtained demonstrate the potential of Fe_3O_4-CA@Au-12-MDA nanoparticles a magnetic SERS platform for the detection of low concentrations of organic dyes.

Keywords: SERS, detection, methylene blue, gold nanoparticles, functionalization, 12-mercaptododecanoic acid, magnetic nanoparticles, Fe_3O_4, Raman spectroscopy, limit of detection.

Introduction

Detection of organic dye molecules at low concentrations is of great importance for environmental monitoring, industrial process control, and analytical chemistry. Synthetic dyes are widely used in various industries, including textile, pharmaceutical, and chemical manufacturing, resulting in their frequent release into aquatic ecosystems. Even at low concentrations, these compounds may persist in the environment and serve as indicators of anthropogenic pollution [1–3].

Among various analytical methods Surface-Enhanced Raman Scattering (SERS) has attracted considerable attention due to its ability to provide highly sensitive and molecule-specific detection through vibrational «fingerprint» signals [4, 5]. Compared with conventional analytical techniques, SERS offers rapid analysis with minimal sample preparation and low operational costs, making it a promising tool for trace detection of organic compounds. Typically, SERS detection involves substrate fabrication, analyte deposition (drop-casting or solution mixing), and signal calibration based on characteristic Raman bands of the target molecule [6–11].

Methylene blue (MB) is widely used as a model analyte in SERS studies due to its well-defined Raman spectrum, chemical stability, and strong affinity toward metallic surfaces [8, 9, 12]. In ecology applications, MB is commonly employed as a model pollutant for evaluating water purification processes and monitoring degradation efficiency in photocatalytic and oxidation systems [13, 14]. Beyond environmental analysis, SERS-based detection of MB has also been investigated in food safety applications, including the analysis of dye residues in biological tissues, as well as in the development of ultrasensitive sensing platforms based on advanced nanomaterials [15–17]. Therefore, reliable detection of methylene blue at low concentrations is not only of analytical interest but also important for evaluating the signal enhancement efficiency of newly developed nanostructured Raman substrates [18, 19].

Over the past decade, various nanostructured materials have been investigated as SERS substrates. Among them, noble metal-based systems, including gold and silver nanoparticles [15, 16], nanorods, and

nanoporous films [20], are the most widely used due to their strong plasmonic properties. In addition, hybrid structures such as metal-semiconductor composites [21–23] including, Au/Cu_2O и Ag/ZnO systems, as well as porous and three-dimensional architectures based on graphene foams, silicon photonic crystals, and nanowires, have demonstrated enhanced sensitivity owing to the increased density of electromagnetic «hot spots» [23–25]. More recently, emerging materials such as two-dimensional MXenes and MoS-based heterostructures [26, 27], together with flexible polymeric and paper-based substrates [17, 28], have further expanded the practical applicability of SERS-platforms.

These developments have enabled progressively lower detection limits. For example, silver nanowire-based substrates demonstrated detection capabilities down to 10^{-16} M [29], whereas various hybrid and porous systems typically operate within the range 10^{-9}-10^{-12} M [24, 30]. Other platforms, including paper-based substrates and metal oxide composites, generally achieve detection limits in the ranges 10^{-8}-10^{-10} M [17, 22]. Despite these advances, a trade-off often exists between sensitivity, reproducibility, structural complexity, and fabrication simplicity. Advanced architectures, including three-dimensional and lithographically patterned nanostructures, provide high structural precision and reproducibility but frequently require technologically complex fabrication procedures [31, 32].

In recent years, FeO-based and Fe_3O_4/Au hybrid nanostructures have attracted attention as magnetic SERS substrates due to the combination of magnetic properties and plasmonic signal enhancement [33–36]. Several studies demonstrated successful SERS detection of rhodamine dyes and other probe molecules using Fe_3O_4-containing composites and Fe_3O_4/Au systems. For example, Fe_3O_4@Au NPs have superior SERS sensitivity for rhodamine and crystal violet with a detection limit of 10^{-7} M [34], magnetically assembled Fe_3O_4@SiO_2@Au structures enabled ultrasensitive detection of rhodamine B and methylene blue down to 1 fM, while Fe_3O_4/Au liquid SERS systems demonstrated enhancement factors (EF) in the range of 10^4-10^7 depending on Au:Fe_3O_4 ratio and external magnetic field conditions[36]. In addition to substrate design, analyte adsorption efficiency plays a critical role in SERS performance. Interactions between target molecules and the substrate surface directly influence signal intensity, particularly at low concentrations [37, 38]. However, insufficient surface affinity remains a limiting factor for reliable detection in many nanoparticle-based systems. Detailed analyses describing the influence of analyte orientation, surface chemistry, and concentration on SERS intensity have been reported previously [39–41]. To address these challenges, surface functionalization strategies aimed at improving analyte localization and signal reproducibility are increasingly being explored [42]. In this context, thiol- and carboxyl-containing ligands represent a promising approach due to their affinity toward metallic surfaces and their ability to introduce functional groups promoting interactions with target molecules [43–46].

In this work, magnetic Fe_3O_4 nanoparticles were functionalized with citric acid followed by gold deposition and subsequent surface modification with 12-mercaptododecanoic acid (12-MDA) to obtain a magnetic SERS-substrate for MB detection. The presence of Au nanostructures and surface carboxyl groups contributed to enhanced Raman signal intensity and improved localization of methylene blue molecules in SERS-regions. The developed substrate enabled MB detection in the concentration range of 10^{-2}-10^{-7} M using a simple nanoparticle-based approach.

Experimental

Reagents: isopropyl alcohol, iron(II) chloride tetrahydrate, iron(III) chloride hexahydrate, hydrogen tetrachloroaurate(III) trihydrate, 12-mercaptododecanoic acid (12-MDA) were purchased from Sigma-Aldrich. Sodium hydroxide, hydrochloric acid (HCl), citric acid (CA), sodium citrate, ammonia, and ethanol were of analytical grade. Deionized water (18.2 MΩ) was prepared using the Akvilon-D 301 (Akvilon JSC, Podolsk, Russian Federation) system.

Preparation of Fe_3O_4-CA@Au nanoparticles was carried out according to the procedure reported in our previous work [47]. The modification scheme is presented in Figure 1.

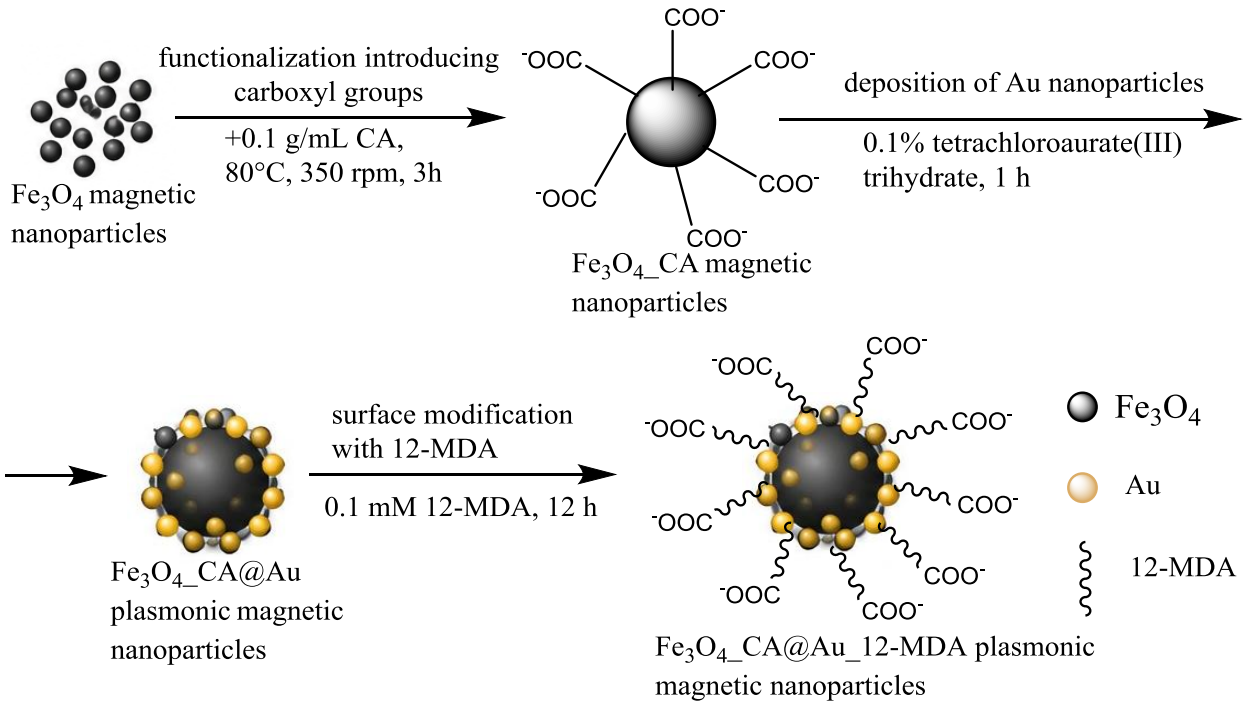

Figure 1. Schematic illustration of the preparation of Fe_3O_4-CA@Au 12-MDA nanoparticles

Preparation of Magnetite Fe_3O_4 Nanoparticles

Fe_3O_4 nanoparticles were synthesized by chemical co-precipitation from aqueous solutions of iron(II) chloride tetrahydrate $FeCl_2 \cdot 4H_2O$ (9.95 g) and iron(III) chloride hexahydrate $FeCl_3 \cdot 6H_2O$ (27.05 g) at a molar ratio of Fe^{3+}:Fe^{2+}=2:1. The synthesis was carried out in acidic medium by adding 11.8 mL of 35 % hydrochloric acid to prevent premature hydrolysis and oxidation of ions Fe^{2+}. The reaction mixture was prepared in 100 mL of deionized water and gradually heated to 60 ºC, under continuous blending. Nanoparticle precipitation was achieved by adding aqueous ammonia solution under intensive stirring until alkaline conditions were reached without heating. After reaching alkaline pH, the reaction mixture was heated at 80-85 ºC for 2 h under argon atmosphere. Under these conditions, intermediate iron hydroxide species formed and subsequently transformed into magnetite.

The obtained magnetic nanoparticles were separated using an external magnet and repeatedly washed with deionized water 5-6 times until neutral pH to remove residual ions and by-products. The nanoparticles were additionally washed with ethanol and dried at 60 ºC for 1h.

Citric Acid Functionalization of Magnetite Fe_3O_4 Nanoparticles and Subsequent Gold Deposition

At the first stage, 2 g Fe_3O_4 nanoparticles were dispersed in 50 mL of deionized water for 15 min using ultrasonication (operating frequency 20-25 kHz, 80 % amplitude, ultrasonic power 900 W). The dispersed nanoparticles were then added to an aqueous citric acid solution 0.1 g/mL and blended at 80 ºC and 350 rpm for 3 h. During this process, citric acid is adsorbed onto the Fe_3O_4 surface through coordination of its carboxylate groups with surface Fe sites. This surface functionalization preserves the crystal structure of magnetite while exposing free carboxyl groups that improve colloidal stability and provide anchoring sites for subsequent gold deposition. As a result, the Fe_3O_4 surface was functionalized with citrate molecules, exposing terminal carboxyl groups that facilitate the adsorption of Au^{3+} ions and subsequent gold deposition.

After modification, the nanoparticles were separated using a magnet, thoroughly washed with deionized water 3-5 times, and air-dried. Subsequently, 1 g of citric acid-modified nanoparticles was dispersed in 0.1 % aqueous solution of hydrogen tetrachloroaurate(III) trihydrate, where Au^{3+} ions interacted with functional groups on the nanoparticle surface.

Reduction of gold ions was performed by adding sodium citrate under heating at 60-70 ºC followed by aging of the reaction mixture for several hours. As a result, nanoparticles Fe_3O_4-CA@Au were formed. The obtained composite particles were separated magnetically, washed with diluted hydrochloric acid and deionized water to remove unbound components, and dried at 60 °C.

Modification of Nanoparticles Fe_3O_4-CA@Au with 12-MDA.

The obtained nanoparticles 0.1 g Fe_3O_4-CA@Au were surface-modified using 12-MDA. For this purpose, the nanoparticles were dispersed in a 0.1 mM 12-MDA, solution prepared in isopropanol (IPA) and stirred at room temperature for 12 h. After completion of the reaction, the nanoparticles were separated using an external magnetic field and repeatedly washed with IPA to remove unbound ligand molecules and residual reagents. As a result, organically modified Fe_3O_4-CA@Au 12-MDA nanoparticles containing surface carboxyl groups were obtained.

Characterization of Samples

Characterization of the obtained nanoparticles was performed at each modification stage: Fe_3O_4, Fe_3O_4-CA@Au и Fe_3O_4-CA@Au-12-MDA. The presence of functional groups on the nanoparticle surface was investigated using Fourier-transform infrared spectroscopy (FTIR) on an InfraLUM FT-08 spectrometer (Lumex, Russia).

The phase composition of the samples was analyzed by X-ray diffraction (XRD) using a SmartLab diffractometer (Rigaku Corporation, Japan).

Morphology and microstructure of the nanoparticles were studied by scanning electron microscopy (SEM), while elemental composition at different modification stages was determined using energy-dispersive X-ray spectroscopy (EDX) on a Hitachi TM 3030 instrument (Hitachi, Japan).

SERS Detection

The obtained Fe_3O_4-CA@Au 12-MDA nanoparticles were used for detection of the model dye MB using an EnSpectr R532 Enhanced Spectrometry. The detection scheme is presented in Figure 2. Silicon substrates were used for deposition of both the dye and nanoparticles. Raman spectra were recorded in the range of 2000-1000 cm^{-1} using laser power values of 28-32, an exposure time of 2000, and 25 scans. Each measurement was performed in triplicate. The calibration curves were constructed using the mean intensity values, and the error bars represent the standard deviation of three independent measurements. The dye concentration range was

10^{-2}–10^{-7} M. The main calibration peaks corresponded to signals at 1625 and 1396 cm^{-1} associated with aromatic vibrations of MB. For the EF calculation, the concentrations of MB used for the SERS and conventional Raman measurements were C_{SERS} =10^{-7} M and C_{Raman} =10^{-2} M, respectively. The SERS enhancement factor (EF) was calculated according to Equation (1):

$$EF = \frac{I_{SERS} / C_{SERS}}{I_{Raman} / C_{Raman}} \quad (1)$$

where I_{SERS} and I_{Raman} — the intensities of characteristic bands in SERS and conventional Raman spectra, respectively, C_{SERS} and C_{Raman} — are the corresponding analyte concentrations. Physically, this concentration-normalized ratio provides an estimate of the Raman signal enhancement relative to the analyte concentration and is primarily associated with the electromagnetic enhancement mechanism arising from localized surface plasmon resonance (LSPR) in the Au-containing nanostructures. Since the exact number of molecules contributing to the SERS signal and the effective surface area of the SERS-active regions were not independently determined, this approach provides an approximate, order-of-magnitude estimation of the EF rather than an absolute value. Therefore, the calculated EF values are used primarily for comparative evaluation of the SERS enhancement performance of the developed substrate.

The limit of detection (LOD) was estimated using the 3σ criterion according to Equation (2):

$$LOD = \frac{3\sigma}{S} \quad (2)$$

where σ — is the standard deviation of three independent measurements at the lowest experimentally tested MB concentration (10^{-7} M), S — is the slope of the corresponding calibration curve. The LOD was estimated separately for the characteristic MB bands at 1623 cm^{-1} and 1396 cm^{-1}.

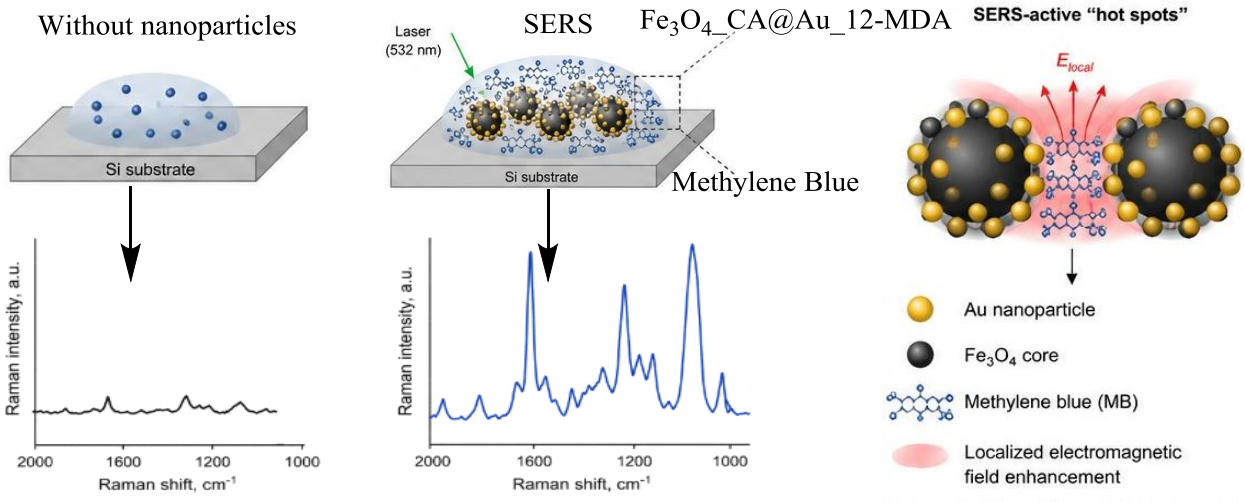

Figure 2. Application of nanoparticles Fe_3O_4-CA@Au 12-MDA as a SERS-substrate for low-concentration detection of MB

Results and Discussion

Nanoparticles before and after modification were investigated by FTIR, SEM-EDX and XRD to evaluate changes in structure, composition, and morphology during the formation of the SERS-substrate.

FTIR analysis was used to confirm modification of Fe_3O_4 nanoparticles with citric acid, subsequent gold deposition, and surface functionalization with 12-MDA. The spectra are presented in Figure 3. FTIR spectra of pristine nanoparticles Fe_3O_4 exhibited characteristic bands corresponding to vibrations Fe-O at 532 cm^{-1}, as well Fe-OH at region 3000-3600 cm^{-1}. In the spectra of samples Fe_3O_4-CA@Au COO^- group vibrations appeared at 1540 cm^{-1} and 1600 cm^{-1} and at region 2500-3600 $см^{-1}$ -OH groups. For Fe_3O_4-CA@Au-12-MDA additional peaks corresponding to C=O groups at 1700 cm^{-1}, as well as symmetric and asymmetric -CH stretching vibrations of the long-chain hydrocarbon fragment of 12-MDA at 2845 cm^{-1} and 2912 cm^{-1}.

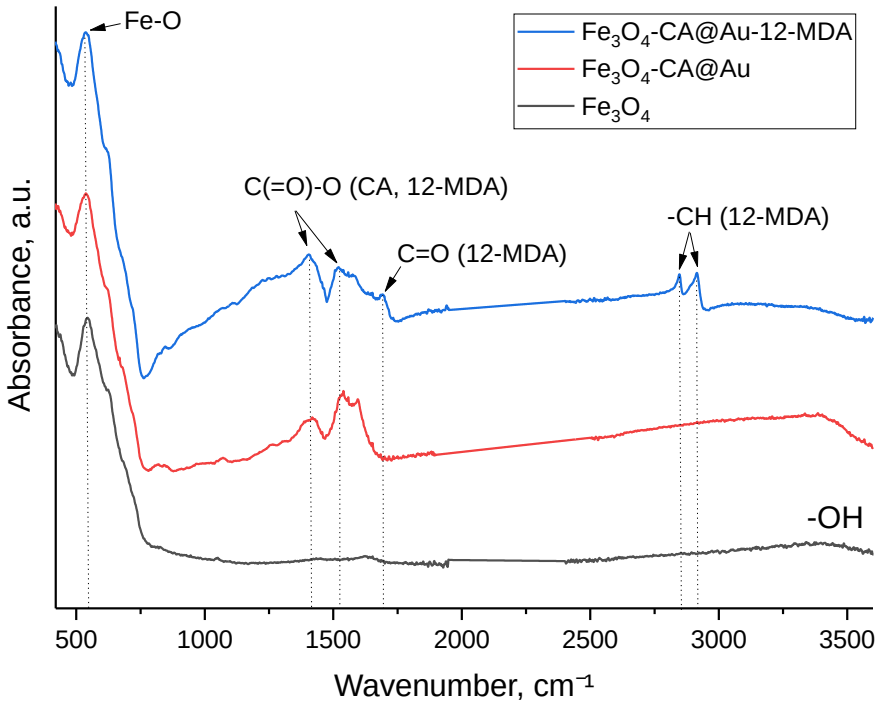

Figures 3. FTIR spectra of nanoparticles before and after modification

XRD analysis was performed to confirm the formation of the magnetic Fe_3O_4 phase and evaluate changes in crystal structure after surface modification and gold deposition. The phase composition of nanoparticles at different modification stages was investigated by X-ray diffraction (Figure 4). Pristine nanoparticles Fe_3O_4 nanoparticles exhibited characteristic diffraction peaks at 2Θ values of 30.2º, 35.5º, 43.2º, 57.1º, 62.7º and 74.2º, corresponding to the (220), (311), (400), (511), (440) and (533) crystallographic planes of magnetite Fe_3O_4, respectively, and these results are in good agreement with literature data and confirm the formation of the cubic spinel structure of magnetite [48]. After gold deposition onto nanoparticles Fe_3O_4-CA@Au additional diffraction peaks appeared at 2Θ values of 38.2º, 44.4º, 64.6º, 77.7º and 81.8º, corresponding to the (111), (200), (220), (311) and (222), planes of metallic gold with a face-centered cubic structure. The appearance of these reflections confirms successful formation of the gold shell on the surface of magnetic nanoparticles.

For samples Fe_3O_4-CA@Au-12-MDA the positions of the main diffraction peaks corresponding to magnetite and gold remained unchanged, while their intensities slightly decreased due to organic surface modification. Nevertheless, these results indicate preservation of the crystal structure of the composite nanoparticles. Furthermore, the absence of additional crystalline phases confirms the high purity of the obtained composite nanoparticles and successful stepwise surface modification without structural degradation during functionalization.

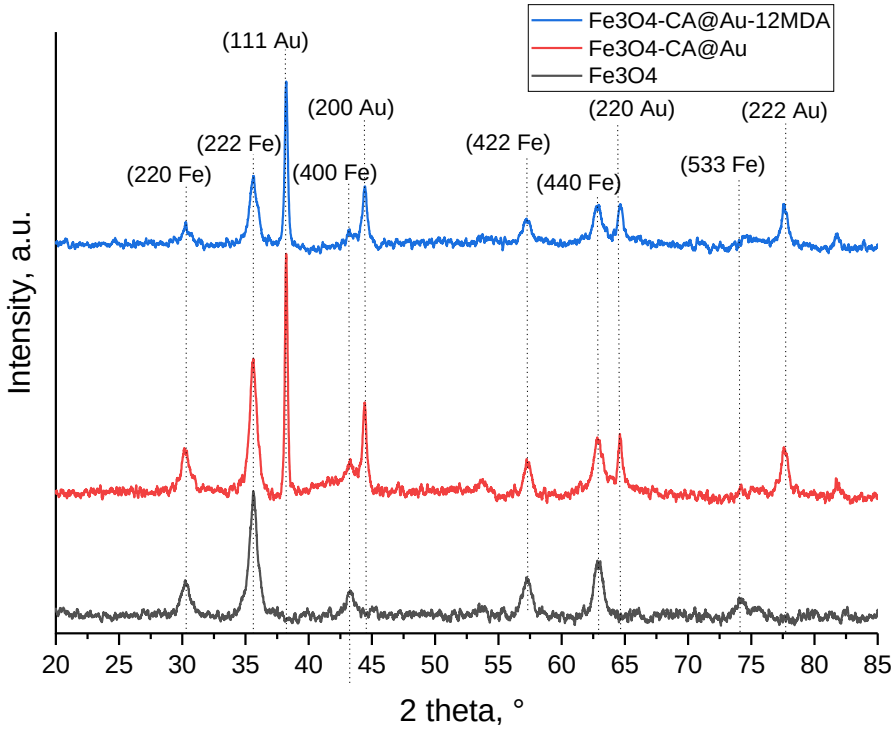

Figure 4. XRD-diffractogram of nanoparticles before and after modification

According to SEM-EDX analysis, the morphology and elemental composition of the obtained nanoparticles were investigated at different modification stages (Figure 5). Pristine nanoparticles Fe_3O_4 exhibited agglomerated irregular-shaped particles. Elemental mapping demonstrated a uniform distribution of Fe and O throughout the particles, while quantitative EDX analysis showed the presence of Fe (76.5 wt %) and O (23.5 wt %). After citric acid functionalization and gold deposition, the surface of Fe_3O_4-CA@Au nanoparticles became rougher, and EDX analysis confirmed the presence of Au (1.2 wt%) and C (14.6 wt %) together with Fe (78.1 wt %) and O (5.4 wt %). A weak sulfur signal (0.7 wt%) was detected in the intermediate Fe_3O_4-CA@Au sample. Considering that no S-containing reagents were used at this stage, this low-intensity signal is most likely attributable to the detection limit of EDX and/or background contamination. Following 12-MDA modification, sulfur (2.2 wt %) was additionally detected in Fe_3O_4-CA@Au-12-MDA samples, while the carbon content increased to 18.5 wt % (Fe 55.8 wt %, O 20 wt %, Au 3.5 wt %), indicating suc-

cessful surface functionalization with thiol-containing ligands. The quantitative elemental compositions of the nanoparticles at different modification stages are summarized in Table S1. It should be noted that the resolution of the obtained images does not allow accurate determination of the nanoparticle size. Nevertheless, the nanoparticles and their gold coating were synthesized using a previously developed method [47], while the successful formation of the obtained nanostructures was additionally confirmed by XRD analysis. The average particle sizes of Fe_3O_4 (21.2 nm) and Fe_3O_4-CA@Au (29.6 nm) reported in [47] were determined by TEM and are cited here for comparison. The increase in the average particle size reported in [47] was attributed to gold deposition on the Fe_3O_4 nanoparticles. It should be noted that the resolution of the SEM images obtained in the present study does not allow reliable determination of the individual nanoparticle size or direct visualization of an Au shell around individual Fe_3O_4 nanoparticles.

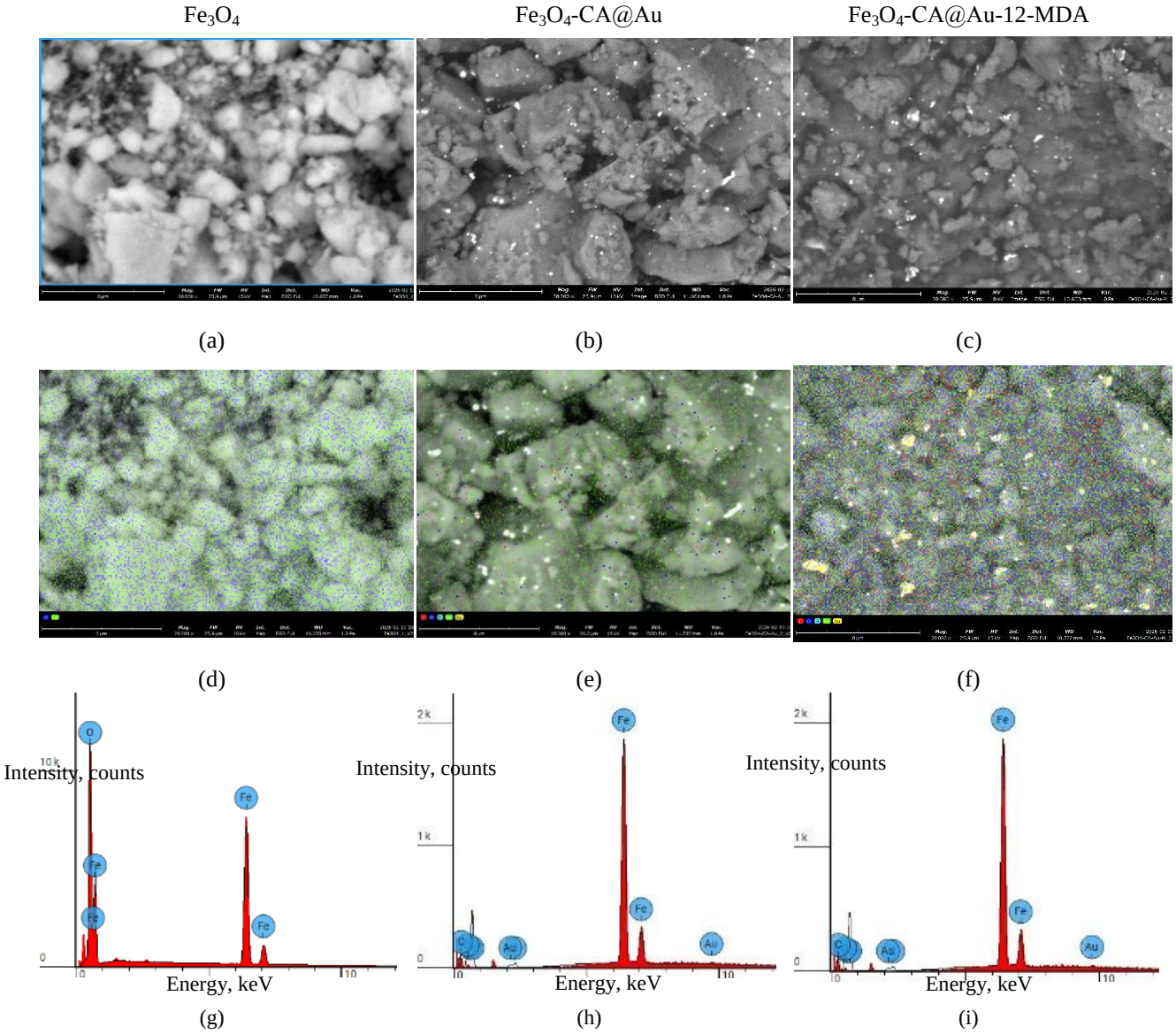

Figure 5. SEM images (a, b, c), EDX elemental mapping (d, e, f), and EDX spectra (g, h, i) of nanoparticles before and after modification

The FTIR, SEM-EDX and XRD results confirmed successful stepwise modification of Fe_3O_4, nanoparticles, gold deposition, and subsequent surface functionalization with 12-MDA. The presence of Au, preservation of the Fe_3O_4 crystal structure, and the introduction of surface carboxyl groups enabled the obtained Fe_3O_4-CA@Au-12-MDA nanoparticles to be used as a SERS-magnetic substrate for methylene blue detection in the concentration range of 10^{-2}-10^{-7} M.

Figure 6 presents Raman spectra of MB recorded without a SERS substrate and in the presence of nanoparticles Fe_3O_4-CA@Au-12-MDA. For samples without nanoparticles, the Raman signal intensity was significantly lower compared with spectra recorded in the presence of nanoparticles, while concentrations of 10^{-7} M were not detected due to the low sensitivity of conventional Raman spectroscopy.

In the presence of Fe_3O_4-CA@Au-12-MDA nanoparticles, substantial enhancement of the MB signal was observed, particularly for the characteristic bands centered at approximately 1620-1628 cm^{-1} and 1392-1400 cm^{-1}, corresponding to aromatic C=C and C-N vibrations, respectively. Compared with the conventional Raman spectrum, a slight shift of the aromatic C=C band was observed in the SERS spectra. This behavior may be associated with the adsorption of MB molecules onto the functionalized Au surface, leading to changes in the local molecular environment and adsorption geometry. Even at concentrations as low as 10^{-7}, characteristic MB bands, including the shifted aromatic C=C band, remained detectable in the presence of the SERS substrate. The intensity of the SERS signal depended on the selected recording area (Figure 7). Characteristic MB peaks were predominantly observed in localized SERS-active regions «hot spots formed in areas of nanoparticle agglomeration (Figure 7b). In regions without pronounced aggregation, the signal intensity was significantly lower or absent. To account for the variability associated with the non-uniform distribution of nanoparticle aggregates, SERS measurements were performed in triplicate. The variability of the SERS response was evaluated using the standard deviation of three independent measurements, which is presented as error bars in the calibration curves (Figure 8). An additional advantage of Fe_3O_4-CA@Au-12-MDA nanoparticles is their magnetic nature, which promoted localization of the analyte droplet without significant spreading across the surface and, consequently, concentration of MB molecules in plasmonically active regions. This likely contributed to enhancement of the local electromagnetic field within nanogaps between closely spaced metallic nanoparticles and increased intensity of the recorded signal.

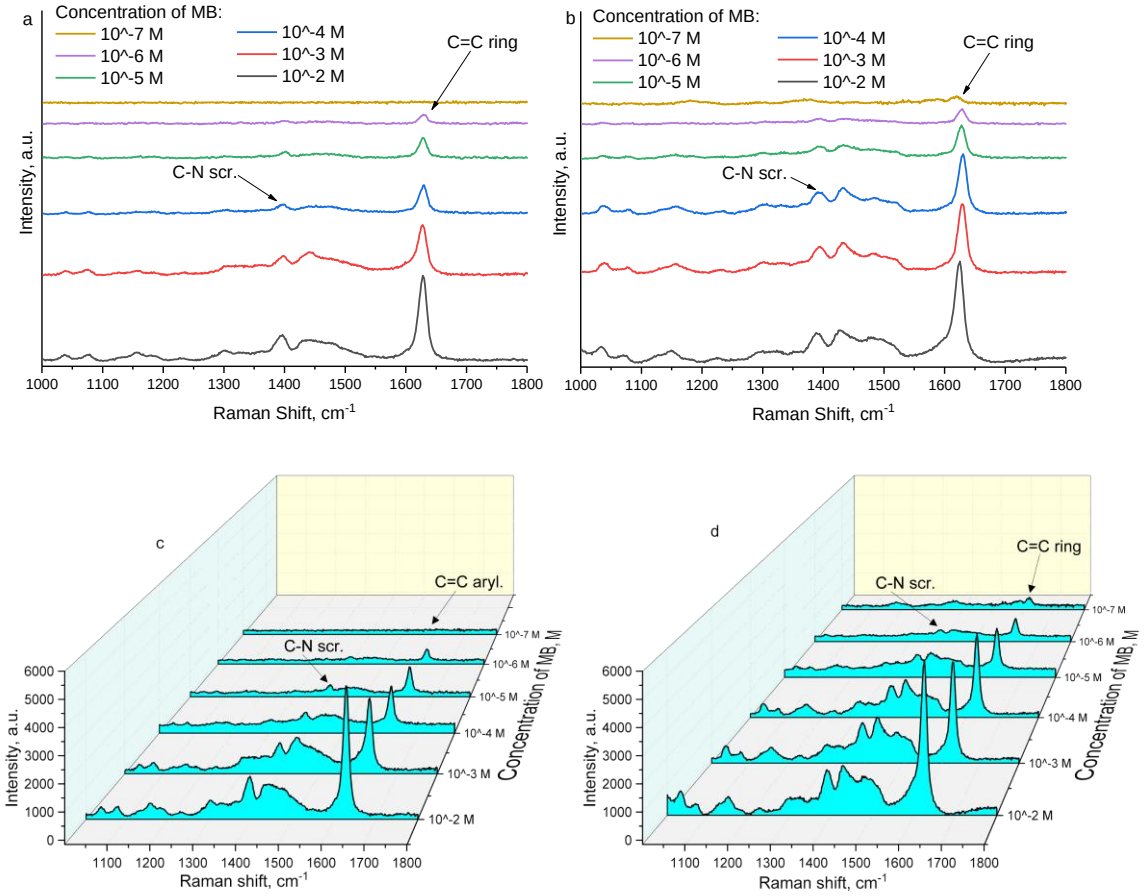

Figure 6. Raman spectra of MB in the concentration range of 10^{-2}-10^{-7} M recorded without a SERS substrate (a, c) and in the presence of a Fe_3O_4-CA@Au-12-MDA -based SERS substrate (b, d)

a b

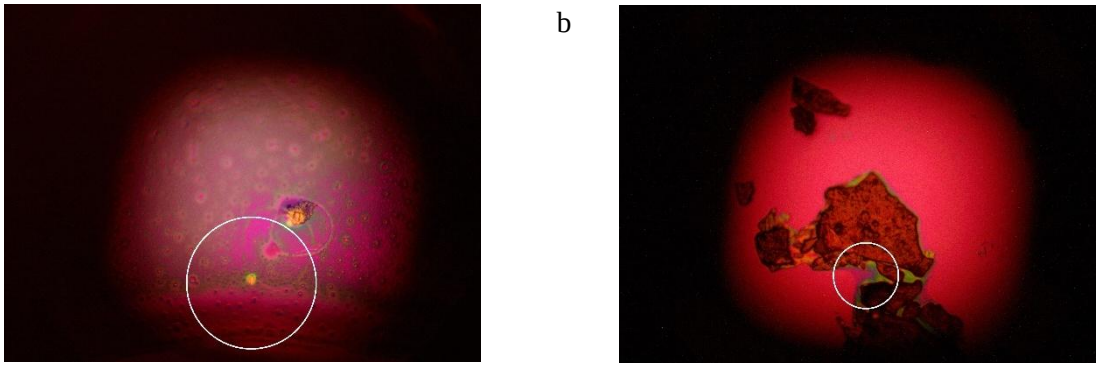

Figure 7. Optical micrographs of regions used for SERS spectrum acquisition of MB on the surface of Fe_3O_4-CA@Au-12-MDA nanoparticles: (a) region without pronounced nanoparticle agglomeration; (b) localized SERS «hot spot» region with nanoparticle agglomeration and dye accumulation

Table 1 and Figure 8 present the analytical parameters and calibration curves for MB detection using conventional Raman spectroscopy and SERS with nanoparticles Fe_3O_4-CA@Au-12-MDA. Calibration curves were constructed based on the intensities of the characteristic MB bands at 1396 и 1623 cm^{-1} in the concentration range of 10^{-2}-10^{-7} M. The calibration data represent the mean values of three independent measurements, with the corresponding standard deviations shown as error bars in Figure 8.

The developed SERS substrate enabled experimental detection of methylene blue down to 10^{-7} M and exhibited good quantitative performance, with R^2 values ranging from 0.98 to 0.99. The LOD values calculated using the 3σ criterion were 4.05×10^{-8} M and 5.97×10^{-8} M for the bands at 1623 and 1396 cm^{-1}, respectively. Thus, 10^{-7} M represents the lowest MB concentration experimentally tested and detected in this study, whereas the calculated values represent the estimated detection limits. The EF for the bands at 1623 and 1396 cm^{-1} were 0.11×10^5 and 0.15×10^5, respectively. These values were calculated by comparing the SERS response at 10^{-7} M MB with the conventional Raman response at 10^{-2} M MB, taking into account the five-order-of-magnitude difference in analyte concentration. The corresponding Raman signal intensity increases were 5.95- and 5.40 times, respectively. Since the exact number of molecules contributing to the SERS signal and the effective surface area of the SERS-active regions were not independently determined, the calculated EF values should be regarded as approximate, order-of-magnitude estimates and are used primarily for comparative evaluation of the developed SERS substrate.

A comparison with previously reported SERS substrates for MB detection is presented in Table 1. The estimated LOD values obtained for Fe_3O_4-CA@Au-12-MDA (4.05×10^{-8} and 5.97×10^{-8} M for the bands at 1623 and 1396 cm^{-1}, respectively) were lower than those reported for the Au@MUA substrate (1.9×10^6-2.3×10^6 M). As expected, Ag-based substrates exhibited considerably higher EF because of the stronger localized surface plasmon resonance of silver nanostructures. Compared with the Au@MUA substrate, the developed Fe_3O_4-CA@Au-12-MDA nanoparticles showed approximately threefold higher EF values 0.11-0.15×10^5 versus 0.4×10^4, while maintaining excellent calibration linearity (R^2 = 0.98-0.99). Although the difference cannot be attributed solely to the replacement of MUA with 12-MDA, since the nanoparticle architecture also differs, the combination of the Fe_3O_4 magnetic core, Au shell, and 12-MDA surface functionalization provides efficient SERS activity together with the practical advantage of magnetic separation and substrate recovery.

Table 1

Comparison of the analytical characteristics of previously reported SERS substrates for methylene blue detection

Sample	Peaks, cm^{-1}	LOD, M	EF	SERS-signal increase, fold	R^2	Ref.
Raman-spectra	1623		1	-	0.94	This work
SERS Fe_3O_4-CA@Au-12-MDA	1623	4.05×10^{-8}	0.11×10^5	5.95	0.98	
Raman-spectra	1396		1	-	0.97	
SERS Fe_3O_4-CA@Au-12-MDA	1396	5.97×10^{-8}	0.15×10^5	5.4	0.99	
MWCNTs-Ag	1395, 1621		4.68×10^6	-	0.99	[49]
Au@MUA	1400, 1625	1.9×10^6-2.3×10^6	0.4×10^4	-	0.93-0.95	[46]

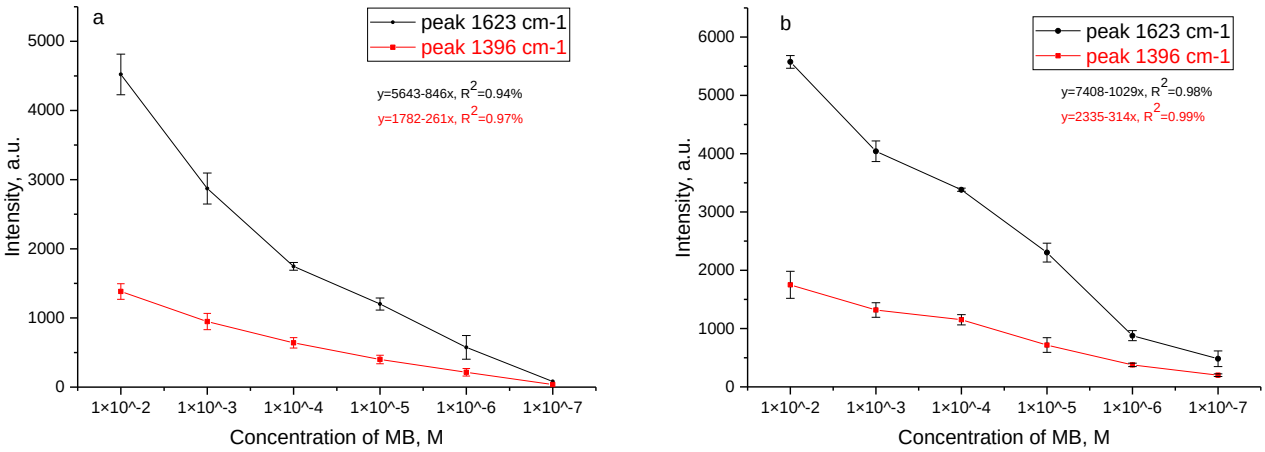

Figure 8. Calibration curves of methylene blue obtained using conventional Raman spectroscopy and SERS Fe_3O_4-CA@Au-12MDA substrates

Conclusions

In this work, Fe_3O_4-CA@Au-12-MDA nanoparticles were obtained for use as a magnetic SERS substrate for MB detection. Stepwise nanoparticle modification was confirmed by FTIR, SEM-EDX and XRD analyses. The obtained results demonstrated preservation of the Fe_3O_4 crystal structure after gold deposition and subsequent organic modification, as well as the presence of Au and carboxyl-containing groups on the nanoparticle surface.

The use of nanoparticles Fe_3O_4-CA@Au-12-MDA as a SERS substrate resulted in enhanced MB signal intensity compared with conventional Raman spectroscopy. The most intense signals were recorded in localized SERS «hot spots» regions associated with nanoparticle agglomeration. The obtained SERS substrates experimental detection of characteristic methylene blue bands in the concentration range of 10^{-2}-10^{-7} M. The estimated LOD values calculated using the 3σ criterion were 4.05×10^{-8} M and 5.97×10^{-8} M for the bands at 1623 and 1396 cm^{-1}, respectively. For the bands at 1623 and 1396 cm^{-1} the approximate EF values were 0.11×10^5 and 0.15×10^5, respectively. In addition, the Raman signal intensities increased by factors of 5.95 and 5.4 respectively, compared with conventional Raman spectroscopy. The constructed calibration curves demonstrated good linearity with R^2 values of 0.98-0.99.

Thus, the obtained Fe_3O_4-CA@Au-12-MDA nanoparticles represent a promising magnetic SERS-platform for detection of low concentrations of organic dye molecules.

Data Availability Statement

The data supporting the findings of this study are available within the article and deposited in Figshare at: https://doi.org/10.6084/m9.figshare.33292149. Further data are available from the corresponding author upon reasonable request.

Funding

This research was funded by the Science Committee of the Ministry of Science and Higher Education of the Republic of Kazakhstan (Grant No. AP23486127, BR28713053).

*Author Information**

**The authors' names are presented in the following order: First Name, Middle Name and Last Name*

Indira Bazarbayevna Muslimova (*corresponding author*) — PhD, Senior Researcher, Technological laboratory of track-etched membranes, Astana branch of the RSE «Institute of nuclear physics» of the Agency of the Republic of Kazakhstan for Atomic Energy, Abylay Khan Avenue, 2/1, 010009, Astana, Kazakhstan; *e-mail: i.muslimova@inp.kz*; https://orcid.org/0000-0002-0923-5506

Ainur Berikkyzy Khairusheva — Master's student, L.N. Gumilyov Eurasian National University, Satpayev street, 2, 010008, Astana, Kazakhstan; e-mail: *ainurkhairusheva@gmail.com*; https://orcid.org/0009-0009-1968-5189

Kairat Aslanbekuly Izbassar — Master's student, L.N. Gumilyov Eurasian National University, Satpayev street, 2, 010008, Astana, Kazakhstan; e-mail: *kaira.kim31@gmail.com*; https://orcid.org/0009-0007-2368-2189

Zhangali Akhmetkaliuly Bekbol — Master's student, L.N. Gumilyov Eurasian National University, Satpayev street, 2, 010008, Astana, Kazakhstan; e-mail: *zhangali.bekbol@mail.ru;* https://orcid.org/0000-0002-8703-0874

Lana Igorevna Lissovskaya — Master of Natural Sciences, Engineer of the Technological laboratory of track-etched membranes, Astana branch of the RSE «Institute of nuclear physics» of the Agency of the Republic of Kazakhstan for Atomic Energy, Abylay Khan Avenue, 2/1, 010009, Astana, Kazakhstan; *e-mail: l.lissovskaya@inp.kz*; https://orcid.org/0000-0002-3894-6366

Ilya Vladimirovich Korolkov — PhD, Leading Researcher, Technological laboratory of track-etched membranes, Astana branch of the RSE «Institute of nuclear physics» of the Agency of the Republic of Kazakhstan for Atomic Energy, Abylay Khan Avenue, 2/1, 010009, Astana, Kazakhstan; *e-mail: i.korolkov@inp.kz*; https://orcid.org/0000-0002-0766-2803

Author Contributions

The manuscript was written through contributions of all authors. All authors have given approval to the final version of the manuscript. CRediT: **Indira Bazarbayevna Muslimova** data curation, investigation, validation, formal analysis, visualization, writing-review, writing-original draft & editing; **Ainur Berikkyzy Khairusheva** methodology, formal analysis; **Kairat Aslanbekuly Izbassar** formal analysis, validation; **Zhangali Akhmetkaliuly Bekbol** formal analysis, validation; **Lana Igorevna Lissovskaya** formal analysis, validation; **Ilya Vladimirovich Korolkov** conceptualization, methodology, supervision, writing-review & editing

Declaration of Generative AI and AI-Assisted Technologies in the Writing Process

During the preparation of this work, the authors used ChatGPT for language editing and grammar improvement of the manuscript. After using this service, the authors carefully reviewed and edited the content and take full responsibility for the final version of the publication.

Conflicts of Interest

The authors declare no conflict of interest.

References

1 Hayat, M., Shah, A., Hakeem, M. K., Irfan, M., Haleem, A., Khan, S. B., & Shah, I. (2022). A designed miniature sensor for the trace level detection and degradation studies of the toxic dye Rhodamine B. *RSC Advances*, *12*(25), 15658–15669. https://doi.org/10.1039/D2RA01722A

2 Koohkan, R., Kaykhaii, M., Sasani, M., & Paull, B. (2020). Fabrication of a Smartphone-Based Spectrophotometer and Its Application in Monitoring Concentrations of Organic Dyes. *ACS Omega*, *5*(48), 31450–31455. https://doi.org/10.1021/ACSOMEGA.0C05123

3 Han, C., Wang, Z., Cui, J., Liu, S., Yang, L., Fu, Y., Zhu, B., & Guo, C. (2025). Rapid Quantitative Detection of Dye Concentration in Pt/TiO2 Photocatalytic System Based on RGB Sensing. *Sensors*, *25*(10), 3195. https://doi.org/10.3390/S25103195

4 Wang, C., Weng, G., Li, J., Zhu, J., & Zhao, J. (2024). A review of SERS coupled microfluidic platforms: From configurations to applications. *Analytica Chimica Acta*, *1296*, 342291. https://doi.org/10.1016/j.aca.2024.342291

5 Chen, B., & Qiu, X. (2025). Surface-Enhanced Raman Scattering (SERS) for exosome detection. *Clinica Chimica Acta*, *568*, 120148. https://doi.org/10.1016/j.cca.2025.120148

6 Pérez-Jiménez, A. I., Lyu, D., Lu, Z., Liu, G., & Ren, B. (2020). Surface-enhanced Raman spectroscopy: benefits, trade-offs and future developments. *Chemical Science*, *11*(18), 4563–4577. https://doi.org/10.1039/D0SC00809E

7 Fan, M., Andrade, G. F. S., & Brolo, A. G. (2020). A review on recent advances in the applications of surface-enhanced Raman scattering in analytical chemistry. *Analytica Chimica Acta*, *1097*, 1–29. https://doi.org/10.1016/J.ACA.2019.11.049

8 Langer, J., de Aberasturi, D. J., Aizpurua, J., Alvarez-Puebla, R. A., Auguié, B., Baumberg, J. J., Bazan, G. C., Bell, S. E. J., Boisen, A., Brolo, A. G., Choo, J., Cialla-May, D., Deckert, V., Fabris, L., Faulds, K., Javier García de Abajo, F., Goodacre, R., Graham, D., Haes, A. J., Liz-Marzán, L. M. (2020). Present and Future of Surface-Enhanced Raman Scattering. *ACS Nano*, *14*(1), 28–117. https://doi.org/10.1021/ACSNANO.9B04224

9 Pilot, R., Signorini, R., Durante, C., Orian, L., Bhamidipati, M., & Fabris, L. (2019). A Review on Surface-Enhanced Raman Scattering. *Biosensors*, *9*(2), 57. https://doi.org/10.3390/BIOS9020057

10 Zhang, Q., Chai, Y., Li, X., Wang, Z., Zhang, X., Effah, C. Y., Ding, L., & Wu, Y. (2026). Surface-enhanced Raman spectroscopy for protein detection: Challenges and countermeasures. *Talanta*, *298*, 128901. https://doi.org/10.1016/j.talanta.2025.128901

11 Lin, S., Nie, Z., Xing, Y., Wang, R., & Yu, F. (2026). SERS detection and antibacterial treatment of bacterial infections. *Coordination Chemistry Reviews*, *546*, 217079. https://doi.org/10.1016/j.ccr.2025.217079

12 Rathod, J., Byram, C., Kanaka, R. K., Bharati, M. S. S., Banerjee, D., Akkanaboina, M., & Soma, V. R. (2022). Hybrid Surface-Enhanced Raman Scattering Substrates for the Trace Detection of Ammonium Nitrate, Thiram, and Nile Blue. *ACS Omega*, *7*(18), 15969–15981. https://doi.org/10.1021/ACSOMEGA.2C01095

13 Anastasopoulos, J. A., Soto Beobide, A., Manikas, A. C., & Voyiatzis, G. A. (2017). Quantitative surface-enhanced resonance Raman scattering analysis of methylene blue using silver colloid. *Journal of Raman Spectroscopy*, *48*(12), 1762–1770. https://doi.org/10.1002/JRS.5233

14 Nguyen, T. Van, Vu, C. D., Pham, T. B., Pham, V. H., Bui, H., Vu, T. H. H., & Pham, V. H. (2021). Detection of Ultra-Low Concentration of Methylene Blue by Porous Silicon Photonic Crystals Covered With Silver Nanoparticles as Efficient Sers Substrate. *Communications in Physics*, *31*(4), 381. https://doi.org/10.15625/0868-3166/15927

15 Li, C., Huang, Y., Lai, K., Rasco, B. A., & Fan, Y. (2016). Analysis of trace methylene blue in fish muscles using ultra-sensitive surface-enhanced Raman spectroscopy. *Food Control*, *65*, 99–105. https://doi.org/10.1016/J.FOODCONT.2016.01.017

16 Xu, T., Wang, X., Huang, Y., Lai, K., & Fan, Y. (2019). Rapid detection of trace methylene blue and malachite green in four fish tissues by ultra-sensitive surface-enhanced Raman spectroscopy coated with gold nanorods. *Food Control*, *106*, 106720. https://doi.org/10.1016/J.FOODCONT.2019.106720

17 Yang, G., Fang, X., Jia, Q., Gu, H., Li, Y., Han, C., & Qu, L. L. (2020). Fabrication of paper-based SERS substrates by spraying silver and gold nanoparticles for SERS determination of malachite green, methylene blue, and crystal violet in fish. *Microchimica Acta*, *187*(5), 310. https://doi.org/10.1007/S00604-020-04262-2

18 Schiavi, S., Taglietti, A., Magni, A., Galinetto, P., & Albini, B. (2025). Increasing SERS performance of silver nanoparticles with nanometric coating of polydopamine: A novel approach for methylene blue detection. *Applied Surface Science*, *687*, 162223. https://doi.org/10.1016/J.APSUSC.2024.162223

19 Tayyaba, N., Zago, S., Giura, A., Fiore, G., Ribotta, L., Scaglione, F., & Rizzi, P. (2025). Nanoporous Copper Films via Dynamic Hydrogen Bubbling: A Promising SERS Substrate for Sensitive Detection of Methylene Blue. *Nanomaterials*, *15*(12), 945. https://doi.org/10.3390/NANO15120945

20 Huh, Y., & Ryu, S. (2025). Ultra-Effective Methylene Blue Detection by Nanoporous Gold for Surface-Enhanced Raman Spectroscopy. *Electronic Materials Letters*, *21*(2), 260–267. https://doi.org/10.1007/S13391-024-00541-9

21 Pham, T. T. H., Vu, X. H., Dien, N. D., Trang, T. T., Chi, T. T. K., Phuong, P. H., & Nghia, N. T. (2022). Ag nanoparticles on ZnO nanoplates as a hybrid SERS-active substrate for trace detection of methylene blue. *RSC Advances*, *12*(13), 7850–7863. https://doi.org/10.1039/D2RA00620K

22 Zamora-Peredo, L., García-Ramirez, J. I., García-Velasco, A. C., Hernández-Torres, J., García-González, L., Bizarro, M., & Báez-Rodríguez, A. (2021). Influence of Ag Photodeposition Conditions over SERS Intensity of Ag/ZnO Microspheres for Nanomolar Detection of Methylene Blue. *Nanomaterials*, *11*(12), 3414. https://doi.org/10.3390/NANO11123414

23 Yang, J., Chen, B., Peng, J., Huang, B., Deng, W., Xie, W., & Luo, Z. (2021). Preparation of CuO Nanowires/Ag Composite Substrate and Study on SERS Activity. *Plasmonics*, *16*(4), 1059–1070. https://doi.org/10.1007/S11468-020-01358-6

24 Ren, S., Fu, J., Liu, G., Zhang, H., Wang, B., & Yu, J. (2025). Ultrasensitive detection of methylene blue by surface-enhanced Raman scattering (SERS) with Ag nanoparticle-decorated magnetic CoNi layered double hydroxides. *Analytical Methods*, *17*(5), 1010–1020. https://doi.org/10.1039/D4AY01841A

25 Srichan, C., Ekpanyapong, M., Horprathum, M., Eiamchai, P., Nuntawong, N., Phokharatkul, D., Danvirutai, P., Bohez, E., Wisitsoraat, A., & Tuantranont, A. (2016). Highly-Sensitive Surface-Enhanced Raman Spectroscopy (SERS)-based Chemical Sensor using 3D Graphene Foam Decorated with Silver Nanoparticles as SERS substrate. *Scientific Reports*, *6*(1), 23733. https://doi.org/10.1038/srep23733

26 Peng, Y., Cai, P., Yang, L., Liu, Y., Zhu, L., Zhang, Q., Liu, J., Huang, Z., & Yang, Y. (2020). Theoretical and Experimental Studies of Ti3C2 MXene for Surface-Enhanced Raman Spectroscopy-Based Sensing. *ACS Omega*, *5*(41), 26486–26496. https://doi.org/10.1021/ACSOMEGA.0C03009

27 Wei, H., Liu, X., Cui, Y., Li, L., Liu, Y., Ma, Y., Li, H., & Xu, Q. (2025). Gold nanobipyramids/MXene@PVDF membrane material for SERS detection and sensitive determination of fluorescent dyes. *Spectrochimica Acta Part A: Molecular and Biomolecular Spectroscopy*, *334*, 125944. https://doi.org/10.1016/J.SAA.2025.125944

28 Sharma, S., Kumar, R., & Yadav, R. M. (2024). Polyacrylonitrile as a versatile matrix for gold nanoparticle-based SERS substrates. *Nanoscale Advances*, *6*(4), 1065–1073. https://doi.org/10.1039/D3NA01112G

29 Horta, I., Neto, N. F. A., Kito, L. T., Miranda, F., Thim, G., Pereira, A. L. de J., & Pessoa, R. (2025). Ultra-Trace Monitoring of Methylene Blue Degradation via AgNW-Based SERS: Toward Sustainable Advanced Oxidation Water Treatment. *Sustainability*, *17*(10), 4448. https://doi.org/10.3390/SU17104448

30 Quan, Y., Su, R., Yang, S., Chen, L., Wei, M., Liu, H., Yang, J., Gao, M., & Li, B. (2021). In-situ surface-enhanced Raman scattering based on MTi20 nanoflowers: Monitoring and degradation of contaminants. *Journal of Hazardous Materials*, *412*, 125209. https://doi.org/10.1016/J.JHAZMAT.2021.125209

31 Guselnikova, O., Lim, H., Kim, H. J., Kim, S. H., Gorbunova, A., Eguchi, M., Postnikov, P., Nakanishi, T., Asahi, T., Na, J., & Yamauchi, Y. (2022). New Trends in Nanoarchitectured SERS Substrates: Nanospaces, 2D Materials, and Organic Heterostructures. *Small*, *18*(25), 2107182. https://doi.org/10.1002/SMLL.202107182

32 Srivastava, K., Le-The, H., Lozeman, J. J. A., van den Berg, A., van der Stam, W., & Odijk, M. (2024). Prospects of nano-lithographic tools for the fabrication of surface-enhanced Raman spectroscopy (SERS) substrates. *Micro and Nano Engineering*, *23*, 100267. https://doi.org/10.1016/J.MNE.2024.100267

33 Du, J., Xu, J., Sun, Z., & Jing, C. (2016). Au nanoparticles grafted on Fe3O4 as effective SERS substrates for label-free detection of the 16 EPA priority polycyclic aromatic hydrocarbons. *Analytica Chimica Acta*, *915*, 81–89. https://doi.org/10.1016/J.ACA.2016.02.009

34 Li, F., Yu, Z., Zhao, L., & Xue, T. (2016). Synthesis and application of homogeneous Fe3O4 core/Au shell nanoparticles with strong SERS effect. *RSC Advances*, *6*(13), 10352–10357. https://doi.org/10.1039/C5RA27875A

35 He, J., Song, G., Wang, X., Zhou, L., & Li, J. (2022). Multifunctional magnetic Fe3O4/GO/Ag composite microspheres for SERS detection and catalytic degradation of methylene blue and ciprofloxacin. *Journal of Alloys and Compounds*, *893*, 162226. https://doi.org/10.1016/J.JALLCOM.2021.162226

36 Hu, F., Lin, H., Zhang, Z., Liao, F., Shao, M., Lifshitz, Y., & Lee, S. T. (2014). Smart Liquid SERS Substrates based on Fe3O4/Au Nanoparticles with Reversibly Tunable Enhancement Factor for Practical Quantitative Detection. *Scientific Reports*, *4*(1), 7204. https://doi.org/10.1038/srep07204

37 Ha Anh, N., Quan Doan, M., Xuan Dinh, N., Quang Huy, T., Quang Tri, D., & Le, A. T. (2022). Gold nanoparticles-based SERS nanosensor for thiram and chloramphenicol monitoring in food samples: Insight into effects of analyte molecular structure on their sensing performance and signal enhancement. *Applied Surface Science*, *584*, 152555. https://doi.org/10.1016/J.APSUSC.2022.152555

38 Vo Huu, T., Tran Nhat, V. T., Xuan, M. N., Thi Ngoc, H. N., Hoang, L. N., Anh, T. D., Huu, K. N., & Le Vu Tuan, H. (2025). Synergistic enhancement of EM and CM in Ag/AZO thin films for high-performance SERS detection of R6G and methylparaben. *RSC Advances*, *15*(19), 14604–14619. https://doi.org/10.1039/D5RA01381J

39 Scher, K. M. R., Wang, Z., Nair, A., Wu, Y., Bartoli, M., Rovere, M., Tagliaferro, A., Rangan, S., Wang, L., & Fabris, L. (2022). Concentration and Surface Chemistry Dependent Analyte Orientation on Nanoparticle Surfaces. *The Journal of Physical Chemistry C*, *126*(38), 16499–16513. https://doi.org/10.1021/ACS.JPCC.2C05007

40 Liu, X., Ye, Z., Xiang, Q., Xu, Z., Yue, W., Li, C., Xu, Y., Wang, L., Cao, X., & Zhang, J. (2023). Boosting electromagnetic enhancement for detection of non-adsorbing analytes on semiconductor SERS substrates. *Chem*, *9*(6), 1464–1476. https://doi.org/10.1016/j.chempr.2023.01.017

41 Liu, C. Y., Cheng, H. W., Lai, M. Y., Tsai, H. M., Liang, M. Y., Biring, S., & Liu, S. W. (2024). Analyte-induced SERS hot spots for dramatically improving the ability to distinguish different concentrations of chemical solutions. *Journal of the Taiwan Institute of Chemical Engineers*, *165*, 105769. https://doi.org/10.1016/J.JTICE.2024.105769

42 Sun, F., Galvan, D. D., Jain, P., & Yu, Q. (2017). Multi-functional, thiophenol-based surface chemistry for surface-enhanced Raman spectroscopy. *Chemical Communications*, *53*(33), 4550–4561. https://doi.org/10.1039/C7CC01577A

43 Renata, S., Verma, N., Tu, Z., Pan, R. L., Hofmann, M., & Lin, C. H. (2021). Development of a tri-functional nanoprobe for background-free sers detection of sialic acid on the cell surface. *Chemosensors*, *9*(5), 92. https://doi.org/10.3390/CHEMOSENSORS9050092

44 Raveendran, J., & Docoslis, A. (2021). Detection and quantification of toxicants in food and water using Ag–Au core-shell fractal SERS nanostructures and multivariate analysis. *Talanta*, *231*, 122383. https://doi.org/10.1016/J.TALANTA.2021.122383

45 Chandran, L., Mohan, A., & Gopchandran, K. G. (2025). Mercaptoundecanoic acid functionalized gold nanoparticles as SERS substrate for the sensing of 6-thioguanine molecules. *Next Research*, *2*(1), 100130. https://doi.org/10.1016/J.NEXRES.2025.100130

46 Khairusheva, A.B., & Korolkov, I.V. (2026). Synthesis and surface functionalization of gold microtubes for SERS detection of dyes. *RSC Advances*, *16*(24), 22204–22215. https://doi.org/10.1039/D6RA01224H

47 Bekbol, Z. A., Izbasar, K. A., Zaboronok, A., Lissovskaya, L. I., Yang, H., Pihosh, Y., Ishikawa, E., Shakirzyanov, R. I., & Korolkov, I. V. (2025). Carborane-Containing Iron Oxide@Gold Nanoparticles for Potential Application in Neutron Capture Therapy. *Nanomaterials*, *15*(16), 1243. https://doi.org/10.3390/nano15161243

48 Ama, O. M., Aigbe, U. O., Anku, W. W., Osibote, O. A., & Pal, K. (2022). Degradation of Methylene Blue Dye and Bisphenol-A Using Expanded Graphene-Polypyrrole-Magnetite Nanocomposite. *Topics in Catalysis*, *65*(19–20), 1745–1754. https://doi.org/10.1007/S11244-022-01626-1

49 Dinh, N. X., Huy, T. Q., Van Vu, L., Tam, L. T., & Le, A. T. (2016). Multiwalled carbon nanotubes/silver nanocomposite as effective SERS platform for detection of methylene blue dye in water. *Journal of Science: Advanced Materials and Devices*, *1*(1), 84–89. https://doi.org/10.1016/J.JSAMD.2016.04.007